

Predictive-Fixed Switching Frequency Technique for Six-Phase Wind Energy Conversion Systems

Jorge RODAS, Raul GREGOR, Magno AYALA, Osvaldo GONZALEZ

Laboratory of Power and Control Systems

Facultad de Ingeniería, Universidad Nacional de Asunción

Luque, CP 2060, Paraguay

E-mail: {jrodas, rgregor, mayala, & ogonzalez}@ing.una.py

ABSTRACT

Considering the ongoing paradigm for the use of more renewable energy sources, wind energy conversion systems are considered mature technologies. The fault tolerance is one of the most sought-to capabilities for wind energy conversion systems. The ability to maintain operation even after an open-phase fault, allows the system operators to maintain energy production, presenting tangible economic benefits, and the inherent redundancy of six-phase machines by providing the desired fault-tolerant capability with no extra hardware. As a result, different control schemes have been developed in the literature considering linear, non-linear and predictive structures. The latter, also known as finite-set model predictive control techniques are distinguished by a variable switching frequency which causes noise, large voltage and current ripples at low sampling frequency. This paper presents a speed control with an enhanced predictive current control technique with fixed switching frequency applied to the six-phase wind energy conversion systems. Simulation results show the efficiency of the proposed technique, demonstrating that it is a viable alternative to conventional predictive controllers.

Keywords: Multiphase induction generator, predictive control, wind energy conversion systems.

1. INTRODUCTION

The development of wind energy conversion systems (WECS) has matured to which it is ready to become generally accepted power generation technology. High-power WECS allow the analysis of new topologies, where multiphase WECS have been subjects of intense research in the last decade [1]. The additional degrees of freedom of the multiphase WECS bring the possibility of the fault-tolerant capability with no extra hardware, which is particularly appreciated in WECS [2], [3]. In order to control the variables of the multiphase WECS, several control strategies have been studied. Some of the most applied methods are the vector control or field oriented control (FOC) with an inner current control loop and the direct torque control (DTC). On one hand, DTC has some disadvantages such as: variable frequency behavior, weakness in torque control at very low speed and torque and flux pulsations due to the hysteresis bands in comparators. On the other hand, FOC has good current behavior, but it contains one speed control loop, one flux control loop, four current control loops and some transformation models for different coordinate frames for the

six-phase case [4]. So, the complexity and cost of the control system is increased.

In this paper, the speed control is performed based on FOC technique whereas the inner current control loop is based on finite-control-set model-based predictive control (FCS-MPC) technique applied to a six-phase induction machine (IM). For the outer speed control loop, a proportional integrator (PI) controller is implemented and the design is based in a technique detailed in [5]. The inner current control loop based on FCS-MPC strategy offers its advantages such as fast transient response and multi-objective control [6], [7]. As the quality of the model of the system has direct influence on the quality of resulting controllers, this paper also includes an enhanced model based on rotor current estimators proposed in [8], [9]. Despite the benefits and constantly improvements in the design of FCS-MPC controllers, it has several issues to solve for researchers, such as the variable switching frequency of this control technique. This paper tackles this issue by the implementation of a fixed switching frequency for the inner predictive current control (PCC) based on the method studied in [10], [11]. The method selected for this paper combines PCC and a pulse-width modulation (PWM) technique which provides the fixed-switching frequency as well as a reduction in the losses of the six-phase IM. Moreover, this technique is easy to extended to conventional and n -phase IM and it only incorporates a small computational burden to the implementation time.

2. MATHEMATICAL MODEL OF THE SIX-PHASE WECS

Traditionally, the mathematical model of the six-phase IM is simplified by using vector space decomposition (VSD) described in [12]. Therefore, the transformation matrix \mathbf{T} , is used to map the six-phase components (i.e. voltages and currents) into three-orthogonal sub-spaces, namely $\alpha - \beta$, $x - y$ and $z_1 - z_2$. A detailed scheme of the system, which consists in an asymmetrical six-phase IM fed by a dc-link (V_{dc}) and a six-phase voltage source inverter (VSI), is provided in Fig. 1. The VSI exhibits a discrete nature, which yields to $2^6 = 64$ possibilities, and 49 different vectors, as shown in Fig. 2. By considering the gating signals arranged in the vector $\mathbf{S} = [S_a, S_b, S_c, S_d, S_e, S_f]$, where $S_i \in \{0, 1\}$, the stator voltages, $\mathbf{U}_{(t)} = [v_{\alpha s}, v_{\beta s}, v_{x s}, v_{y s}]$, can be obtained from the ideal VSI model $\mathbf{M}_{[\mathbf{S}]}$ as:

$$\mathbf{U}_{(t)} = V_{dc} \mathbf{T} \mathbf{M}_{[\mathbf{S}]} \quad (1)$$

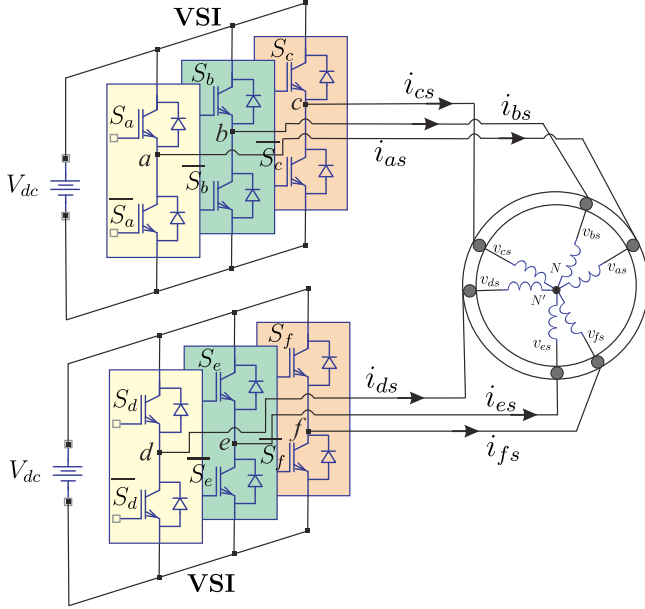
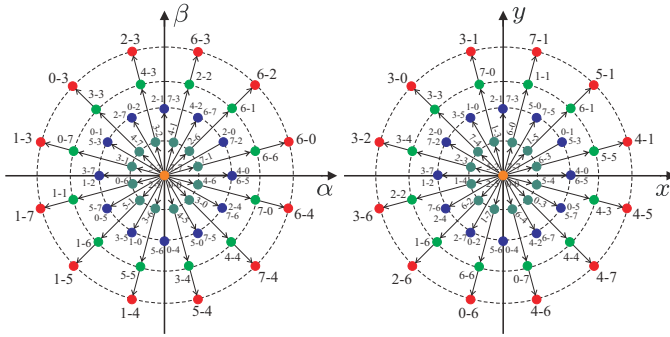


Fig. 1. Scheme of the six-phase IM fed by two 2-level VSI.


 Fig. 2. Space voltage vectors and switching states in the $\alpha - \beta$ and $x - y$ sub-spaces for a six-phase VSI.

$$\mathbf{T} = \frac{1}{3} \begin{bmatrix} a & d & b & e & c & f \\ 1 & \frac{\sqrt{3}}{2} & -\frac{1}{2} & -\frac{\sqrt{3}}{2} & -\frac{1}{2} & 0 \\ 0 & \frac{1}{2} & \frac{\sqrt{3}}{2} & \frac{1}{2} & -\frac{\sqrt{3}}{2} & -1 \\ 1 & -\frac{\sqrt{3}}{2} & -\frac{1}{2} & \frac{\sqrt{3}}{2} & -\frac{1}{2} & 0 \\ 0 & \frac{1}{2} & -\frac{\sqrt{3}}{2} & \frac{1}{2} & \frac{\sqrt{3}}{2} & -1 \\ 1 & 0 & 1 & 0 & 1 & 0 \\ 0 & 1 & 0 & 1 & 0 & 1 \end{bmatrix} \begin{matrix} \alpha \\ \beta \\ x \\ y \\ z_1 \\ z_2 \end{matrix} \quad (2)$$

where an amplitude invariant criterion was used.

$$\mathbf{M}_{[s]} = \frac{1}{3} \begin{bmatrix} 2 & 0 & -1 & 0 & -1 & 0 \\ 0 & 2 & 0 & -1 & 0 & -1 \\ -1 & 0 & 2 & 0 & -1 & 0 \\ 0 & -1 & 0 & 2 & 0 & -1 \\ -1 & 0 & -1 & 0 & 2 & 0 \\ 0 & -1 & 0 & -1 & 0 & 2 \end{bmatrix} \mathbf{S}^T \quad (3)$$

being modeled as the ideal six-phase VSI for two isolated neutrals configuration.

Then, by using a state-space representation, the model of the system is given by:

$$\dot{\mathbf{X}}(t) = \mathbf{A}(t) \mathbf{X}(t) + \mathbf{B}(t) \mathbf{U}(t) + \mathbf{H} \varpi(t) \quad (4)$$

$$\mathbf{Y}(t) = \mathbf{C} \mathbf{X}(t) + \nu(t) \quad (5)$$

being $\mathbf{U}(t)$ the input vector of the state-space system, $\mathbf{X}(t) = [i_{\alpha s}, i_{\beta s}, i_{x s}, i_{y s}, i_{\alpha r}, i_{\beta r}]^T$ the state vector, $\mathbf{Y}(t) = [i_{\alpha s}, i_{\beta s}, i_{x s}, i_{y s}]$ the output vector and $\mathbf{A}(t)$ and $\mathbf{B}(t)$ are matrices related on the electrical parameters of the machine. The process noise is represented by $\varpi(t)$, \mathbf{H} is the noise weight matrix, $\mathbf{C} = [1, 1, 1, 1]$ and $\nu(t)$ the measurement noise. A detailed explanation of the machine model is not included here for the sake of conciseness and can be found in [11].

3. PROPOSED CONTROL METHOD

A. Outer speed control

A PI controller with a saturator is selected for the speed control loop, which is based on the indirect vector control technique because of its simplicity. For this technique, the PI speed controller is used to obtain the dynamic reference current $i_{q s}^*$. This current reference, which will be used by the PCC, is generated from the electric angle estimation used to transform the current reference, originally in the dynamic reference frame $d - q$, to the $\alpha - \beta$ sub-space. The process of the slip frequency (ω_{sl}) estimation is executed in the same way as the indirect field orientation methods, from the electrical parameters of the six-phase IM ($L_r = 3L_m + L_{lr}$ and R_r) and the reference currents in the dynamic reference frame ($i_{d s}^*$, $i_{q s}^*$).

B. Inner predictive current control

The current control is performed by FSC-MPC approach. This PCC technique uses the model of the system, Eqs. (1)-(5), to predict for each valid switching state of the six-phase VSI the performance of the variables to be controlled at every sampling time. Therefore, the model of the system must be discretized. A forward Euler model approximation is used:

$$\hat{\mathbf{X}}_{[k+1|k]} = \mathbf{X}_{[k]} + f(\mathbf{X}_{[k]}, \mathbf{U}_{[k]}, T_s, \omega_r[k]) \quad (6)$$

being T_s the sampling time and $[k]$ the current sample. As the computation of the control signal requires high computational cost, which is comparable with T_s , so a second-ahead of prediction of the variables is required for delay compensation. This second-ahead prediction is implemented and the rotor current is estimated by using rotor current estimator based on Kalman filter recently proposed in [8], [9].

C. Cost function

Once the second-step ahead prediction is obtained, an optimization process is applied every sampling period, where a cost function is minimized by a determined premise. The cost function is considered to evaluate the stator currents tracking by the quadratic error of the $\alpha - \beta$ (related to energy conversion)

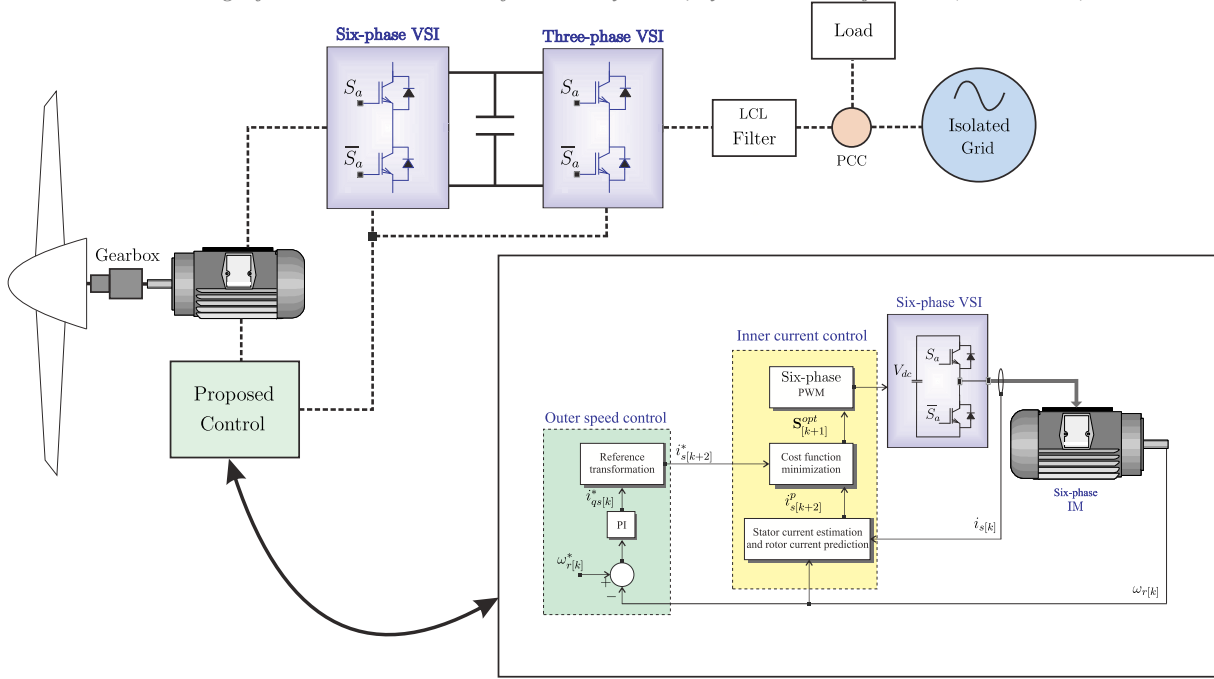


Fig. 3. Block diagram of the proposed speed control with the predictive-fixed current control.

and $x - y$ (related to Joule losses) sub-spaces of the system as follows:

$$g_j[k+2|k] = \left(i_{\alpha s}^*[k+2] - i_{\alpha s}^p[k+2] \right)^2 + \left(i_{\beta s}^*[k+2] - i_{\beta s}^p[k+2] \right)^2 + \lambda_x \left(i_{x s}^*[k+2] - i_{x s}^p[k+2] \right)^2 + \lambda_y \left(i_{y s}^*[k+2] - i_{y s}^p[k+2] \right)^2 \quad (7)$$

where g_j is the cost function of each combination voltage space vector (see Fig. 2), λ_x and λ_y are tuning parameters which give more importance to $\alpha - \beta$ or $x - y$ sub-space, $i_s^*[k+2]$ is a vector containing the reference for the stator currents and $i_s^p[k+2]$ is the second-ahead predicted stator currents.

D. PCC-fixed implementation

The PCC technique determines an optimal vector \mathbf{S}^{opt} through the minimization of the cost function in (7). Then, the PWM method uses the optimal vector and the VSD theory to calculate the duty cycles as follows:

$$\tau = \frac{1}{2} + \frac{3}{4} \mathbf{M}_{[\mathbf{S}^{opt}]} \quad (8)$$

where $\tau = [\tau_a, \tau_b, \tau_c, \tau_d, \tau_e, \tau_f]^T$ and $\mathbf{M}_{[\mathbf{S}^{opt}]}$ is the ideal six-phase VSI model with the optimal vector selected. The duty cycles, presented as τ , are related with the VSI output and are normalized between 0 and 1. This procedure can be analyzed as a systematic application in one sampling period of the optimal combination of the optimal vector and a null vector in order to minimize the stator current error in $\alpha - \beta$ and $x - y$ sub-spaces [11].

E. Optimizer

The proposed predictive model needs to include all 64 possibilities to consider all possible voltage vectors. But Fig. 2 shows the redundancy of the switching space vectors by showing only 49 different vectors (48 active and 1 null). This approach is commonly considered as the optimal solution. Now, for a generic multiphase machine, where n is the phase number and ε is the search vector space (49 for the six-phase IM), the proposed optimization algorithm generates the optimal switching signal set \mathbf{S}^{opt} and then it applies a modulation technique based on PWM to obtain a fixed switching frequency response.

Algorithm 1 Proposed optimization of the algorithm

1. **comment:** Algorithm initial values.: $g_{j_o} := \infty, i := 1$
2. **while** $i \leq \varepsilon$ **do**
3. $\mathbf{S}_i \leftarrow \mathbf{S}_{i,j} \forall j = 1, \dots, n$
4. **comment:** Calculate the stator voltages. Eqn. (1).
5. **comment:** Calculate the prediction of the measurement stator current states Eqn. (6).
6. **comment:** Calculate the prediction of the unmeasurable rotor current states applying the method proposed in [8], [9].
7. **comment:** Calculate the second-ahead prediction of the stator currents $\hat{\mathbf{X}}_{[k+2|k]}$.
8. **comment:** Minimize the cost function. Eqn. (7).
9. **if** $g_j < g_{j_o}$ **then**
10. $g_{j_o} \leftarrow g_j, \mathbf{S}^{opt} \leftarrow \mathbf{S}_i$
11. **end if**
12. $i := i + 1$
13. **end while**
14. **comment:** Calculate the modulation indices through the selected optimal vector. Eqn. (8).

TABLE I
ELECTRICAL AND MECHANICAL PARAMETERS

Six-phase IM			
PARAMETER	SYMBOL	VALUE	UNIT
Stator resistance	R_s	0.62	Ω
Rotor resistance	R_r	0.63	Ω
Stator inductance	L_{ls}	0.0064	H
Rotor inductance	L_{lr}	0.0035	H
Magnetizing inductance	L_m	0.0666	H
System inertia	J_i	0.27	kg·m ²
Viscous friction coefficient	B_i	0.012	kg·m ² /s
Nominal frequency	f_a	50	Hz
Number of pole pairs	p	3	—
Electrical Power	P_w	15	kW

4. SIMULATION RESULTS

A MATLAB/Simulink simulation program has been designed for a six-phase IM fed by a six-phase VSI in order to analyze the proposed PCC with fixed switching frequency for WECS. Numerical integration using first order Euler’s discretization method has been applied to compute the evolution of the state-space variables in the time domain. Table I presents the mechanical and electrical parameters for the six-phase IM. The mean squared error (MSE) and the total harmonic distortion (THD) have been used as indices of performance for the controller. The MSE is computed as:

$$MSE(i_{\phi_s}) = \sqrt{\frac{1}{N} \sum_{j=1}^N (i_{\phi_s} - i_{\phi_s}^*)^2} \quad (9)$$

where N is the number of samples, i_{ϕ_s} the measured stator currents, $i_{\phi_s}^*$ the stator current references and $\phi \in \{\alpha, \beta, x, y\}$. As for the THD is computed as follows:

$$THD(i_s) = \sqrt{\frac{1}{i_{s1}^2} \sum_{j=2}^N (i_{sj})^2} \quad (10)$$

being i_{sj} the harmonic stator currents and i_{s1} the fundamental stator current.

The efficiency of the proposed PCC technique for the six-phase IM has been tested, under a fixed load torque. For every case, a sampling frequency of 10 kHz, the clock modulator frequency equivalent to 1 MHz, a torque load of 15 Nm and a fixed dynamic reference current ($i_{ds}^* = 1$ A) have been used. In Fig. 4 it is shown the switching voltage output for phase a in a period of time and a THD analysis of i_{α_s} , which presents the harmonics amplitude values, highlighting the values for the frequency switching and its multiples. Fig. 5 shows the trajectories of the measured stator currents in the $\alpha - \beta$ and $x - y$ sub-spaces for a reference amplitude of 9.13 A and a frequency of 9.7 Hz.

Then in Fig. 6, it is shown results regarding the rotor speed tracking and the stator currents behavior. The six-phase IM was tested with a low speed of 200 rpm connected to a torque load of 15 Nm. The stator currents show a stable behavior, even in the transient condition. For a efficiency analysis, it was

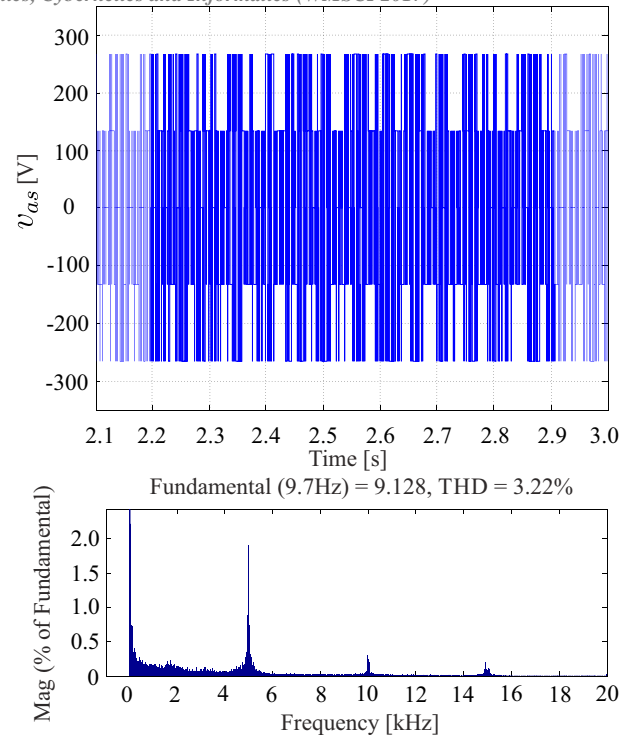


Fig. 4. THD analysis of the measured current i_{α_s} . Simulation results for current amplitude of 9.13 A and a frequency of 9.7 Hz.

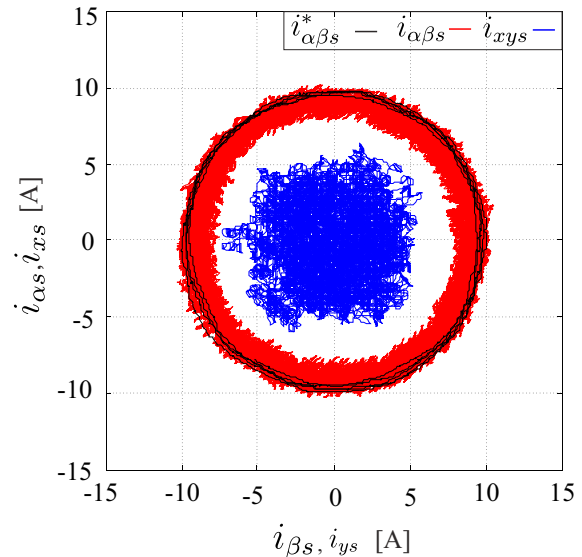


Fig. 5. Stator currents in $\alpha - \beta$ and $x - y$ sub-spaces for current frequency of 9.7 Hz and an amplitude of 9.13 A.

calculated the MSE to show that the proposed algorithm has an optimal response for low speed conditions and a connected full load. The obtained MSE, for a fixed speed reference of 200 rpm, are 0.7891 A, 0.7481 A and 0.845 rpm for i_{α_s} , i_{β_s} and ω_r , respectively. Finally in Fig. 7, it is presented a rotor speed tracking with a reversal condition, showing the response of the speed control algorithm and the PCC tracking of the stator currents in the $\alpha - \beta$ sub-space.

The authors would like to thank to the Paraguayan Government for the economical support through a CONACYT grant project called 14-INV-101.

6. REFERENCES

- [1] M. Duran and F. Barrero, "Recent advances in the design, modeling and control of multiphase machines: Part II," *Industrial Electronics, IEEE Transactions on*, Vol. 63, No. 1, pp. 459–468, Jan. 2016.
- [2] E. Levi, "Advances in converter control and innovative exploitation of additional degrees of freedom for multiphase machines," *Industrial Electronics, IEEE Transactions on*, Vol. 63, No. 1, pp. 433–448, Jan. 2016.
- [3] J. Rodas, H. Guzman, R. Gregor, and F. Barrero, "Model predictive current controller using Kalman filter for fault-tolerant five-phase wind energy conversion systems," in *Proc. 7th PEDG*, Vancouver, Canada, 2016, pp. 1–6.
- [4] F. Barrero and M. Duran, "Recent advances in the design, modeling and control of multiphase machines: Part I," *Industrial Electronics, IEEE Transactions on*, Vol. 63, No. 1, pp. 449–458, Jan. 2016.
- [5] L. Harnefors, S. Saarakkala, and M. Hinkkanen, "Speed control of electrical drives using classical control methods," *Industry Applications, IEEE Transactions on*, Vol. 49, No. 2, pp. 889–898, Mar.-Apr. 2013.
- [6] S. Vazquez, J. Rodriguez, M. Rivera, L. Franquelo, and M. Norambuena, "Model predictive control for power converters and drives: Advances and trends," *Industrial Electronics, IEEE Transactions on*, Vol. 64, No. 2, pp. 935–947, Feb. 2017.
- [7] G. Mirzaeva, G. Goodwin, B. McGrath, C. Teixeira, and M. Rivera, "A generalized MPC framework for the design and comparison of VSI current controllers," *Industrial Electronics, IEEE Transactions on*, Vol. 63, No. 9, pp. 5816–5826, Sep. 2016.
- [8] J. Rodas, F. Barrero, M. Arahal, C. Martin, and R. Gregor, "Online estimation of rotor variables in predictive current controllers: A case study using five-phase induction machines," *Industrial Electronics, IEEE Transactions on*, Vol. 63, No. 9, pp. 5348–5356, Sep. 2016.
- [9] J. Rodas, C. Martin, M. Arahal, R. Gregor, and F. Barrero, "Influence of covariance-based ALS methods in the performance of predictive controllers with rotor current estimation," *Industrial Electronics, IEEE Transactions on*, Vol. 64, No. 4, pp. 2602–2607, Apr. 2017.
- [10] R. Gregor, J. Rodas, J. Munoz, M. Ayala, O. Gonzalez, and D. Gregor, "Predictive-fixed switching frequency technique for 5-phase induction motor drives," in *Proc. SPEEDAM*, Capri, Italy, 2016, pp. 1–7.
- [11] M. Ayala, J. Rodas, R. Gregor, J. Doval-Gandoy, O. Gonzalez, M. Saad, and M. Rivera, "Comparative study of predictive control strategies at fixed switching frequency for an asymmetrical six-phase induction motor drives," in *Proc. IEMDC*, Miami, FL, USA, 2017, pp. 1–8.
- [12] Y. Zhao and T. Lipo, "Space vector PWM control of dual three-phase induction machine using vector space decomposition," *Industrial Electronics, IEEE Transactions on*, Vol. 31, No. 5, pp. 1100–1109, Sep./Oct. 1995.

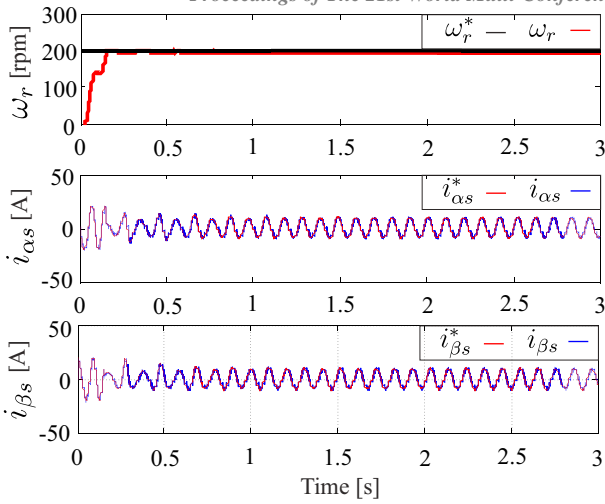


Fig. 6. Simulation results for a fixed speed reference ω_r^* condition of 200 rpm.

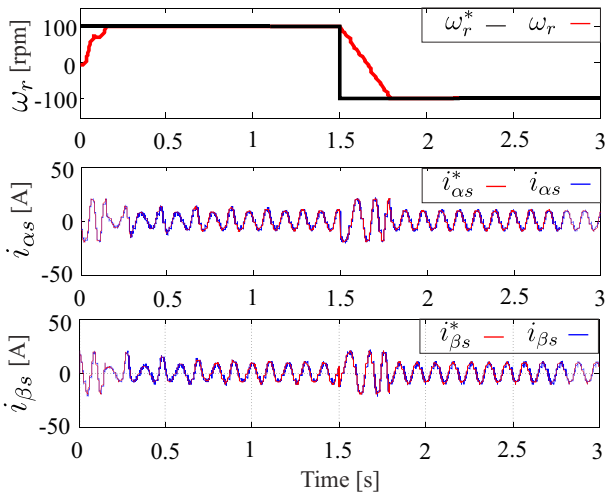


Fig. 7. Simulation results for a fixed speed reference ω_r^* of 100 rpm and a reversal condition.

5. CONCLUSION

In this paper, a speed control with an inner predictive-fixed current predictive control is proposed. One of the main disadvantages of traditional finite-control-set model-based predictive controller is its variables switching frequency. This paper solves this issue by combining the predictive controller with a pulse width modulator. The efficiency of the proposed method is confirmed by the presented simulation results. The proposed controller exhibits excellent performances in steady state as well as in dynamic process. Furthermore, the average switching frequency of the proposed method is even lower than the conventional predictive controller, which means smaller switching losses. Considering that the proposed controller only introduces the computation of the duty cycles, the extension to conventional and n -phase cases is easier than other conventional methods.